LUND UNIVERSITY

Anomalous Protein-Protein Interactions in Multivalent Salt Solution

Pasquier, Coralie; Vazdar, Mario; Forsman, Jan; Jungwirth, Pavel; Lund, Mikael

Anomalous Protein-Protein Interactions in Multivalent Salt Solution

Coralie Pasquier,[*,†] Mario Vazdar,[‡] Jan Forsman,[†] Pavel Jungwirth,[¶] and Mikael Lund[*,†]

Department of Theoretical Chemistry, Lund University, POB 124, SE-22100 Lund, Sweden , Rudjer Bošković Institute, Division of Organic Chemistry and Biochemistry, POB 180, HR-10002 Zagreb, Croatia, and Institute of Organic Chemistry and Biochemistry, Czech Academy of Sciences, Flemingovo nam. 2, 16610 Prague 6, Czech Republic

E-mail: coralie.pasquier@teokem.lu.se; mikael.lund@teokem.lu.se

Phone: +46-46-222 82 51; +46-46-222 86 48

---

[*]To whom correspondence should be addressed

[†]Department of Theoretical Chemistry, Lund University, POB 124, SE-22100 Lund, Sweden

[‡]Rudjer Bošković Institute, Division of Organic Chemistry and Biochemistry, POB 180, HR-10002 Zagreb, Croatia

[¶]Institute of Organic Chemistry and Biochemistry, Czech Academy of Sciences, Flemingovo nam. 2, 16610 Prague 6, Czech Republic

Abstract

The stability of aqueous protein solutions is strongly affected by multivalent ions, which induce ion-ion correlations beyond the scope of classical mean-field theory. Using all-atom Molecular Dynamics (MD) and coarse grained Monte Carlo (MC) simulations, we investigate the interaction between a pair of protein molecules in 3:1 electrolyte solution. In agreement with available experimental findings of "reentrant protein condensation", we observe an anomalous trend in the protein-protein potential of mean force with increasing electrolyte concentration in the order: (i) double-layer *repulsion*, (ii) ion-ion correlation *attraction*, (iii) over-charge *repulsion*, and in excess of 1:1 salt, (iv) non Coulombic *attraction*. To efficiently sample configurational space we explore hybrid continuum solvent models, applicable to many-protein systems, where weakly coupled ions are treated implicitly, while strongly coupled ones are treated explicitly. Good agreement is found with the primitive model of electrolytes, as well as with atomic models of protein and solvent.

Introduction

The stability of protein suspensions, which is at the core of many biotechnological applications, is determined by inter-protein interactions. Among the factors influencing those interactions, the concentration and the nature of the ions present in solution is of a particular importance. The classic way of representing interactions in protein solutions is by using the Derjaguin-Landau-Verwey-Overbeek (DLVO) theory, which takes into account the influence of ions through the Debye length. However, DLVO theory is known to to fail in the case of multivalent counterions.[1,2] Several experimental findings have proven this, one of which being the charge inversion phenomenon: a charged macromolecule (*macroion*) in an oppositely charged multivalent "ions" (*Z-ions*) solution can bind enough ions to *reverse* the sign of its own net charge.[3,4] This has been observed for a variety of macromolecules and ions, such as latex particles, polyelectrolytes, DNA, proteins, multivalent ions and surfactant micelles.[4–13] The mechanism relies mainly on strong spatial correlations between ions adsorbed at the surface of the macromolecule, a feature which is not taken into account by generic mean-field theories.[1–3,14–16]

Human Serum Albumin (HSA) is a 585 residues long, 66.5 kDa protein, which is involved in the transport of diverse molecules in blood plasma.[17] HSA solutions undergo reentrant condensation upon addition of trivalent salts (YCl_3, $LaCl_3$, $FeCl_3$, or $AlCl_3$).[18–20] That is, upon increase of the trivalent salt concentration, protein aggregation is first observed, then redissolution of the samples occurs. This anomalous trend, caused by charge reversal, has been shown to be able to induce clustering, liquid-liquid phase separation or crystallization.[12,18,21–25] The ability to control the phase behavior of protein dispersions show promising opportunities, for example for the production of high quality protein crystals, required for protein structure determination.
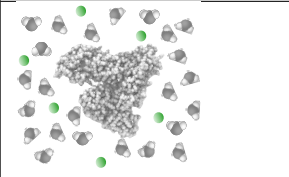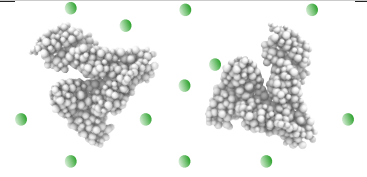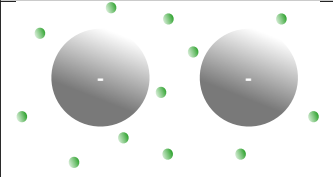
Here, we investigated the interactions between yttrium (Y^{3+}) ions and HSA molecules, as well as how yttrium modulates HSA-HSA interactions, using numerical simulations with three different models: an all-atom model, a coarse-grained model, and a colloidal model.

3

Using different levels of detail enabled us to probe the specificity of the interaction between Y^{3+} and the carboxylic groups of HSA, as well as the protein charge reversal occurring with increasing Y^{3+} concentration (related to reentrant condensation), and the influence of monovalent ions on the Y^{3+}-HSA and HSA-HSA interaction free energy.

Methods

To study ion-protein, protein-protein, and colloid-colloid interactions we use three levels of molecular detail – see Table 1 for an overview. Statistical mechanical averages for each model are obtained using either Molecular Dynamics (MD) or Monte Carlo (MC) simulations as described below.

Table 1: Simulation models used to study ion-protein, protein-protein, and colloid-colloid interactions in 3:1 electrolyte solution.

	Atomic Model	Coarse Grained Model	Colloidal Model
Technique	Molecular Dynamics	Monte Carlo	Monte Carlo
Ensemble	NPT	NVT	NVT
N_{total}	$\mathcal{O}(10^5)$	$\mathcal{O}(10^3)$	$\mathcal{O}(10^2)$
$N_{macromol}$	1	1–2	2
Solvent	Explicit	Implicit	Implicit
Trivalent Ions (•)	Explicit	Explicit	Explicit
Monovalent Ions	Explicit	Implicit / Explicit	Implicit / Explicit

Atomic Protein Model

We performed 100 ns molecular dynamics (MD) simulations (after 1 ns of equilibration) of a single HSA molecule (PDB: 1N5U[26]), described with the OPLS/AA force field,[27] in 0.5 M aqueous solution of YCl_3. The unit cell contained one protein molecule, neutralized by 262 Y^{3+} cations[28] and 767 Cl^- anions, and 29093 SPC/E[29] water molecules. The initial

box length was approximately 10 nm. To approximately account for electronic polarizability, a charge-scaling procedure was adopted and all ions were scaled by $1/\sqrt{\varepsilon_{el}} = 0.75$, ε_{el} being the electronic (high-frequency) dielectric constant of water.[30,31] Electroneutrality of the system was kept by a modification of N-terminus and C-terminus charge of the protein. Periodic boundary conditions were used with long range electrostatic interactions beyond the nonbonded cutoff of 10 Å accounted for using the particle-mesh Ewald procedure[32] with a Fourier spacing of 1.2 Å. The Nose-Hoover thermostat[33] and Parrinello-Rahman[34] barostat with temperature of 298 K (independently controlled for protein and water phase) and pressure of 1 atm was used. The LINCS algorithm[35] was employed to constrain all bonds containing hydrogen atoms, while all water bond lengths were constrained using the SETTLE method.[36] The time step was 2 fs and all MD simulations were performed with GROMACS 4.0.7.[37]

Coarse Grained Protein Model

The atomic HSA structure is coarse grained to the amino acid level where each residue is treated as a soft sphere that can be either neutral or charged, depending on the type of amino acid and the solution pH. The pH is 7.0 in all simulations, giving a protein net charge of $-8.0e$. The solvent is a dielectric continuum while trivalent cations are included explicitly. For sampling the angularly averaged two-body protein-protein distribution function, $g(r)$, the remaining monovalent counter-ions, $N_c = Z_{prot}N_{prot} + 3N_{tri}$, are accounted for via the Debye screening length, $\lambda_D = 1/\kappa = (\epsilon_0\epsilon_r k_B T/N_c V^{-1})^{1/2}$. Previous studies on electric double layers have shown that this mixed description of explicit and implicit salt is in good agreement with the exact solution to the primitive model.[38] The Hamiltonian is composed of an electrostatic and a Lennard-Jones part,

$$\beta\mathcal{H} = \sum_{i}^{N-1}\sum_{j=i+1}^{N}\frac{\lambda_B z_i z_j e^{-\kappa r_{ij}}}{r_{ij}} + 4\beta\varepsilon_{ij}\left[\left(\frac{\sigma_{ij}}{r_{ij}}\right)^{12} - \left(\frac{\sigma_{ij}}{r_{ij}}\right)^{6}\right] \tag{1}$$

5

where N is the number of interaction sites, $\beta = 1/k_B T$ is the inverse thermal energy, $\lambda_B = \beta e^2/4\pi\epsilon_0\epsilon_r = 7.12$ Å is the Bjerrum length at $T = 298.15$ K, r_{ij} is the distance between the ith and jth particle, e is the elementary charge, ϵ_0 is the vacuum permittivity, ϵ_r is the relative permittivity of the medium, ε_{ij} is the depth of the LJ potential, and σ_{ij} is the finite distance at which the inter-particle potential is zero. The Lorentz-Berthelot mixing rule is applied so that $\varepsilon_{ij} = \sqrt{\varepsilon_{ii}\varepsilon_{jj}}$, and $\sigma_{ij} = (\sigma_{ii} + \sigma_{jj})\,/\,2$. The $\sigma_{ii/ij}$ values for protein residues and ions are given in Table 2. For the former, the parameters have been obtained by fitting to experimental virial coefficients for lysozyme and they, without further adjustment, well represent phase equilibria of concentrated protein *mixtures*.[39] The salt parameters reproduce experimental activity coefficients in bulk electrolyte solution up to molar concentration,[40] and for the particular value of $\sigma_{Y^{3+}COO^-}$, please refer to the section "Results and Discussion - Ion-Protein Surface Interaction". This relatively simple, semi-empirical Hamiltonian allows us to use experimental constraints to, on average, maintain a realistic balance between electrostatics and short-range attraction between the proteins. The latter may incorporate van der Waals and hydrophobic interactions and, of course, for improved quantitative agreement, or for strongly hydrophobic proteins, a more advanced Hamiltonian could be applied.

Table 2: Lennard-Jones parameters used for the coarse grained protein and salt model. Radii, $\sigma_{ii}/2$, of amino acid residues are estimated from their molecular weights, M_w, using $\rho = 1$ g/mol/Å^3, and range between 3.3–4.6 Å.

	$\sigma_{ii/ij}$ (Å)	$\varepsilon_{ii/ij}$ ($k_B T$)	Reference
Residues	$(6M_w/\pi\rho)^{1/3}$	0.05	[39]
Y^{3+}COO$^-$	2.2	1.6	see text
Na$^+$	3.8	0.005	[40]
Cl$^-$	3.4	0.005	[40]

Two proteins along with varying amounts of trivalent salt are placed in a cylindrical cell[41] ($L = 563$ Å, $R = 50$ Å) with periodic ends and hard sides, such that the final protein concentration is 50 mg/ml, matching the experimental conditions of ref.[12] Configurations in the canonical ensemble are sampled with the Metropolis Monte Carlo algorithm using ion translations and combined translational/rotational cluster moves of the proteins includ-

ing trivalent ions within 6 Å from the protein surface.[42] The proteins are only allowed to rotate/translate along the z-axis of the cylinder, while the ions are free. Decreasing the cylinder length to radius ratio, L/R, threefold (larger R, smaller L) while maintaining a constant volume, have negligible effects on sampled properties.

The angularly averaged two-body protein-protein distribution function, $g(r)$, is sampled via the histogram method and subsequently used to estimate the protein-protein potential of mean force (PMF) by Boltzmann inversion, $w(r) = -k_B T \ln g(r) + C$ where the free energy of the reference state, C, is chosen such that $w(r) \to 0$ for larger r.

For the total charge calculation, a *single*, static protein is centered in a spherical simulation cell ($R = 81$ Å) such that the protein concentration is 50 mg/ml. Yttrium, chloride, and monovalent protein counterions (Na^+) are explicitly included ($\kappa = 0$) and only ions are allowed to move. The number of charges in spherical shells of increasing radius is averaged throughout the simulation.

All CG protein simulations were performed using the Faunus framework.[43] The electronic Python Notebook (Jupyter) used for running the two-body simulations and construct the presented PMF plots is accessible at `https://github.com/mlund/SI-proteins_in_ multivalent_electrolyte`.

Colloidal Model

Two spherical particles of valency $Z = -42$ as well as their monovalent counterions and 3:1 salt, were confined in a cylinder of length 700 Å, and radius 120 Å. The valency was calculated so that the *surface charge density* would be similar for the colloidal particles and the coarse-grained proteins. The confining surface of the cylinder was hard, but otherwise inert. All simple ions were modelled as charged, hard spheres, with a common hard-sphere diameter, $d = 4$ Å. A non-electrostatic soft repulsion, V was imposed between ions and particles, with $\beta V(r) = (d/(r - R))^9$, for $r > R$. A hard core interaction was also imposed to ensure that the ions did not approach the particles closer than $R + d/2 = 18$ Å. This

7

also defines the inverse surface charge density of the colloids to -97 $\text{Å}^2/e$, which is high but not unusual in colloidal systems. Two different salt concentrations, c_s, as measured by the number of trivalent ions divided by the free volume (or occupied by the particles) inside the cylinder, were considered: $c_s = 0.525$ mM and $c_s = 6.51$ mM. The most dilute system thus only contained 10 trivalent ions, i.e. these were not abundant enough to neutralize the particle charge (though the monovalent counterions did, of course). In the more concentrated system, however, there was, in this sense, an excess of trivalent ions.

We compared our results from this explicit ion model, with corresponding ones in a model where simple monovalent ions were treated implicitly, i.e. in a system with screened Coulomb interactions between multivalent species, with κ established from the monovalent ion concentration, as previously described. However, we must then consider that there are at least two different ways to interpret the cylinder model representation. One may either envisage this as a model of a dispersion in which the overall particle concentration matches that in the cylinder, i.e. about 0.105 mM. It is then appropriate to include the monovalent counterion concentration, contained inside the cylinder, in the calculation of the Debye screening length. On the other hand, one could also envisage our system as a model of how two colloidal particles interact in the limit of infinite dilution, in which case the potential of mean force is directly transferable to the second virial coefficient. In this case, the cylinder boundaries are "superficial", i.e. only a computational necessity. This would imply that our model improves with cylinder size, but also that the counterions would be diluted away in the macroscopic limit. In this case, it is more appropriate to disregard any contribution from the counterions to the Debye screening length. We considered both options in our screened Coulomb model.

Results and Discussion

Ion-Protein Surface Interactions

In this section we first use atomistic and coarse grained simulations to study the distribution of trivalent cations on the surface of HSA. As shown in Figure 1, strong Coulomb interactions between multivalent cations and anionic groups, cause Y^{3+} to associate specifically with negatively charged carboxyl groups on the protein surface. Despite large differences in model granularity and computational complexity, this result is captured by both all atom and coarse grained simulations. The Y^{3+} binding can be quantified by calculating the potential of mean force (PMF) with carboxyl groups, see Figure 2 where we note that the depth of the attractive well is consistent with experimental association constants of ethanoic acid and yttrium, pK ~-1.7 or -3.9 $k_B T$.[44] The Lennard-Jones parameters $\sigma_{Y^{3+}COO^-}$ and $\varepsilon_{Y^{3+}COO^-}$ used in the coarse-grained model have been fitted so that the closest contact as well as the integral $\int_{\text{contact}}^{\infty}(e^{-\beta w(r)}-1)r^2 dr$ for the potential between yttrium ions and carboxylic groups are identical for MD and MC.

Note that the presence of explicit solvent molecules in the atomistic model gives rise to oscillations due to packing which are necessarily absent in the implicit solvent model.
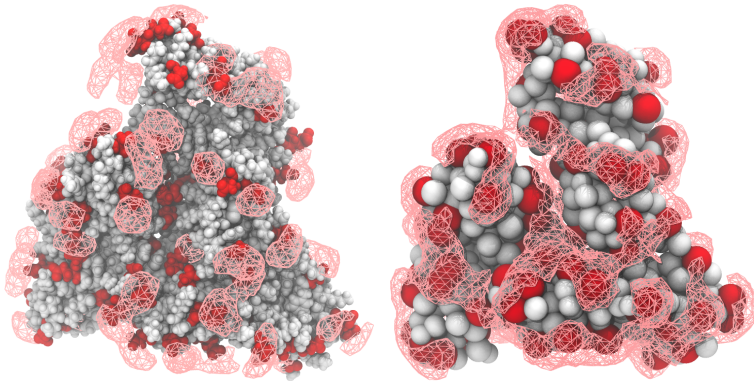

Figure 1: Spatial distribution of trivalent yttrium ions around HSA at a 0.5 mol/l YCl$_3$ concentration. Anionic surface groups are shown in red. *Left:* From atomistic MD. *Right:* From coarse grained MC where each amino acid is represented by a sphere and solvent and monovalent ions are treated implicitly (see Table 1).
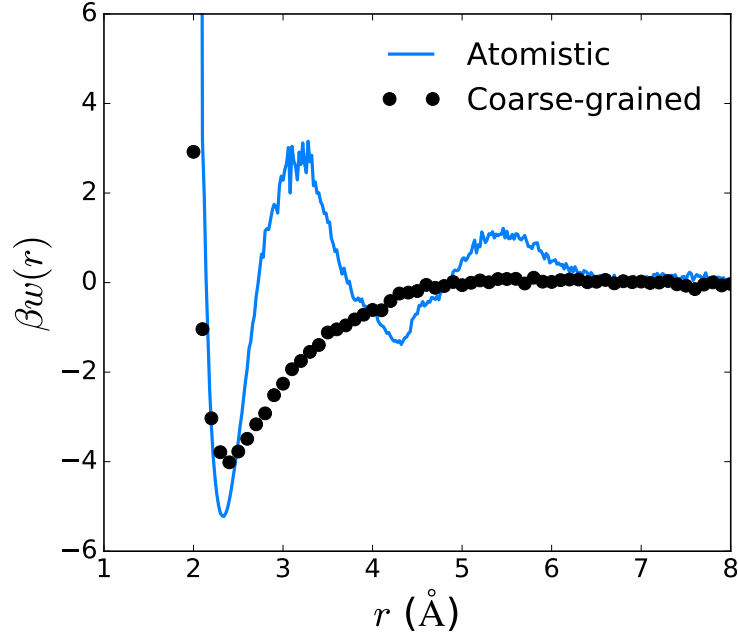
Figure 2: Potential of mean force between Y^{3+} and HSA carboxyl groups as obtained from all atom MD simulations and coarse grained MC. The coarse grained LJ parameters between a trivalent cation and the deprotonated carboxyl group are $\sigma_{Y^{3+}COO^-}$=2.2 Å and $\beta\epsilon_{Y^{3+}COO^-}$=1.6.

We next calculated the total charge of a single HSA molecule with its bound ions at different YCl_3 concentrations. Figure 3 presents the sum of the charges of the protein and the ions (Y^{3+}, Cl^-, and Na^+) present in the smallest spherical shell containing all of the protein plus one ion diameter (a total of 51 Å), at different YCl_3 concentrations. According to the work of Zhang and collaborators,[12] we can estimate the Y^{3+} concentration corresponding to the clouding (c^*) and de-clouding (c^{**}) of a 50 mg/ml HSA solution. They are also reported on figure 3.

We first see a decrease of the absolute value of the charge, caused by the absorption of the yttrium ions on the surface of the negatively charged protein. The neutralization point corresponds perfectly to that reported in the literature for HSA solutions in the presence of YCl_3, that is, c^*.[12] Futher increase of YCl_3 causes the total charge to become increasingly positive, until a maximum around 18 mM. For higher concentrations of YCl_3, we notice a decline of the total charge. The reason is a progressive loss of preferential binding of yttrium
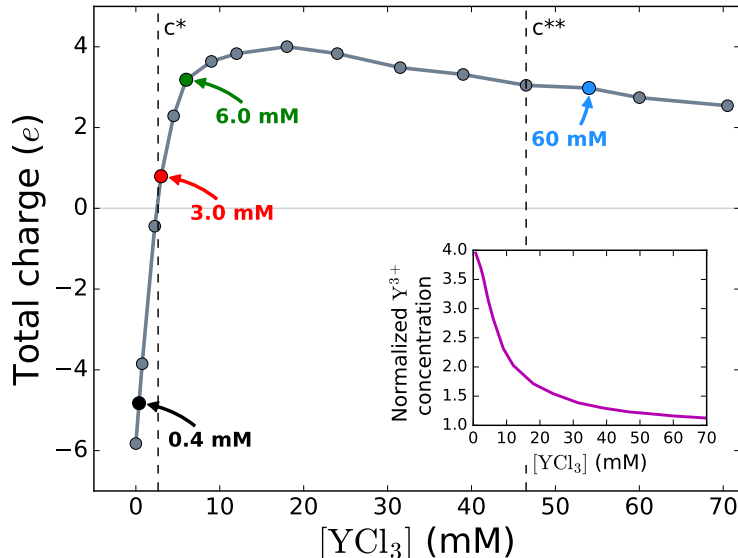
10

Figure 3: Total charge contained in a 51 Å spherical shell, as a function of YCl_3 concentration. The YCl_3 concentrations corresponding to the clouding (c*) and de-clouding (c**) of 50 mg/ml HSA solutions[12] are drawn in dashed lines. The inset shows the yttrium concentration inside the shell normalized by the bulk concentration, as a function of the YCl_3 concentration.

to the protein surface, as shown in the inset of Figure 3. Indeed, the concentration of yttrium close to the protein surface approaches the bulk concentration with increasing YCl_3.

We can interpret this as the loss of electrostatic interactions between the protein surface and yttrium ions, and between yttrium ions themselves, as a consequence of the increasing screening. We can also relate this to the previous simulations of colloids in the presence of trivalent salt,[14] where it was shown that, in an excess of monovalent salt, the amount of overcharging is decreased. Although our system is slightly different (the amount of monovalent coions (Cl^-) increases, but not the amount of monovalent counterions (Na^+), we can imagine a similar phenomenon happening.

Protein-Protein Interactions

Having studied the binding of trivalent ions to the surface of a single HSA molecule we now turn to the self-association between two protein bodies. Using MC simulations we sample the

angularly averaged pair-correlation function, $g(r)$, between two HSA molecules at different yttrium(III) chloride concentrations, and deduce the inter-protein potential of mean force, $w(r)$. As seen on the left graph of Fig. 4, when the concentration of trivalent salt is low (0.4 mM), there is a long-range repulsion ($w(r) > 0$) and a short range attraction ($w(r) < 0$). The former is due to electrostatic monopole-monopole repulsion (protein net charge of $-8e$) in the relatively unscreened solution. The short range attraction is a result of residue-residue van der Waals interactions and, possibly, from higher order electrostatic multipolar moments. Addition of YCl_3 quickly screens the repulsive barrier, inducing attraction and producing a -2 $k_B T$ well in $w(r)$. Further addition of YCl_3 reduces the attractive part and eventually leads to repulsion. At the highest YCl_3 concentrations (60 mM), all attraction disappears and the potential is fully repulsive.
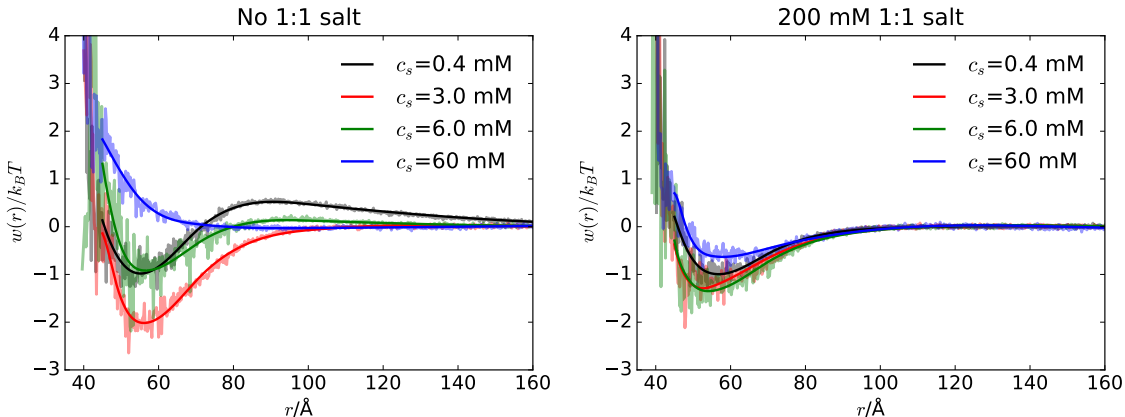
Figure 4: Protein-protein potential of mean force, $w(r)$, as a function of protein mass center separation, r, with increasing yttrium chloride concentration. *Left:* With YCl_3 only. *Right:* With 200 mM added implicit NaCl. Raw simulation data are shown in light colors and are overlaid with fitted splines (solid lines). The curves corresponding to the YCl_3 concentrations used in Fig. 3 have matching colors.

To check if the dampening of the attraction and subsequent repulsion at high YCl_3 concentration was due to overcharging of HSA, or by simple screening, which would lead to a loss of electrostatic attraction and a predominance of steric repulsion at high ionic strength, we performed the same simulation with an added 200 mM ionic strength (accounted for implicitely). The results are shown on the right graph of Fig. 4. In this case, the initial

repulsion at $[\text{YCl}_3] = 0.4$ mM and the attraction at $[\text{YCl}_3] = 3.0$ mM are strongly reduced, showing the importance of the electrostatic component of the HSA-HSA interactions. More importantly, there is no increase of the repulsion at high YCl_3 concentration. Indeed, the screening suppresses the overcharging effect, and only the non-electrostatic component of the protein-protein interaction, that is, the Lennard-Jones attractive part, is present.

The above results correlate well with the reentrant condensation of HSA in the presence of yttrium reported in the litterature.[12,18,23] Indeed, the increase in YCl_3 concentration first causes a reduction of the absolute value of the net charge of HSA molecules, decreasing inter-particle repulsion and promoting inter-particle attraction, whereafter the net charge of the HSA molecules reverses and its absolute value increases, causing renewed repulsion.

In a recent work[45] calorimetry measurements showed that the binding of trivalent ions to the protein surface, and the resulting protein-protein attraction are entropically driven. At first glance, this may seem irreconcilable with the electrostatic energy term in Eq. 1, but it should be observed that in a dielectric continuum solvent, the Coulomb potential is *effective* and implicitly contains solvent degrees of freedom. This is reflected in a temperature dependent relative dielectric constant, $\epsilon_r(T)$, which leads to the counter intuitive result that *entropy* drives two oppositely charged ions together. Using experimental data for the dielectric temperature dependence of water, we have previously shown that ion-ion correlation attraction between like-charged macro-ions in trivalent electrolyte is indeed driven by water entropy.[46] In the following we now focus on macro-ions to illustrate some generic effects of ion-ion correlations and of the model approach taken.

Colloid-Colloid Interactions

In the last section we treated salt using a hybrid model with both implicit and explicit mobile ions. We now investigate the validity of this approach for spherical, charged colloids in the primitive model of electrolytes, i.e. with all ions are included explicitly, in comparison with models where monovalent ions are included implicitly via the Debye screening length. In the

latter case, we either did or did not take into account the counterions of the colloids for the calculation of the total concentration of monovalent ions.

Interparticle free energies at the higher salt concentration, $c_s = 6.5$ mM, are shown in Figure 5.b. In this case, the counterion contribution is almost negligible, and we find excellent agreement between explicit and implicit ion approaches, although the former results naturally displays slightly more noise. At such high concentrations of trivalent ions, correlation attractions dominate at short separations. On the other hand, at low salt concentrations, results from different approaches and models differ considerably - cf Figure 5.a.

Electrostatic screening by simple monovalent ions seems to be underestimated by both implicit approaches. This means that the implicit ion model in which the counterions are included (finite particle concentration model) provides results that agree better with the explicit ion results. However, we should then keep in mind that at such low salt concentrations, the explicit ion results are most likely sensitive to the system (cylinder) size, i.e. our results do not truly represent the dilute particle limit.

One obvious limitation of the current system size, when viewed as a model for the infinite dilute limit, is that the total trivalent ion charge is considerably lower than the particle charge. This can certainly be true in experimental systems, but not in the limit of vanishing particle concentration.
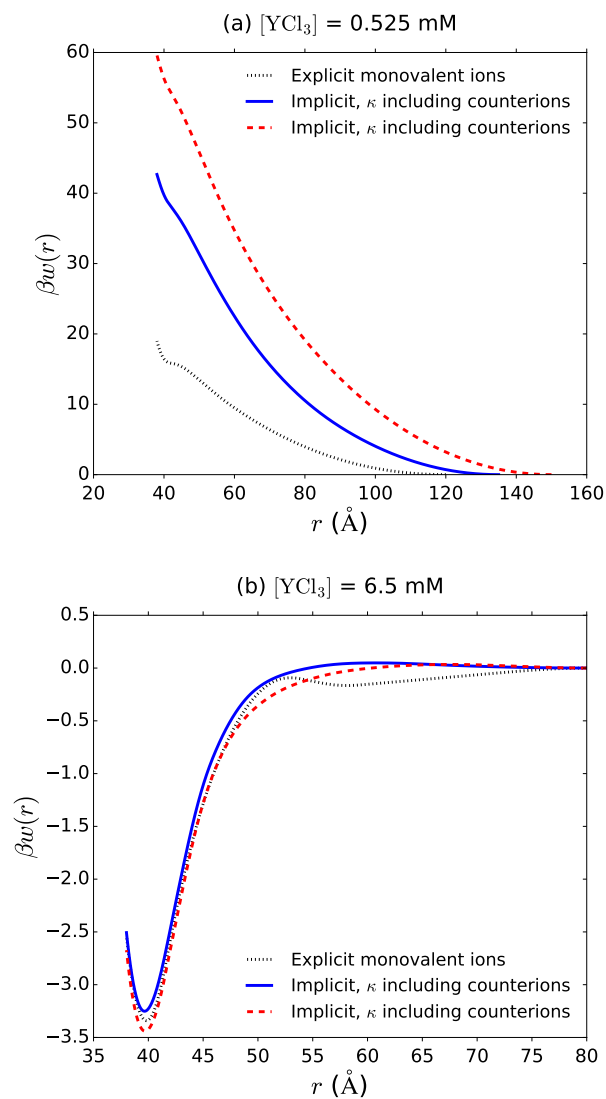
Figure 5: Free energies between two charged particles, contained in a cylinder, at salt concentration of $c_s \approx 0.525$ (a) and $c_s \approx 6.5$ mM (b). Results for the all-explicit ion model, as well as for our two implicit ion models are included (see text for details).

15

Conclusion

We studied the binding of Y^{3+} to Human Serum Albumin (HSA) and its influence on protein-protein interactions. This work, at a microscopic level, echoes experimental results showing the existence of reentrant condensation in HSA solutions in the presence of trivalent ions [18–20] and is also in agreement with recent calorimetry experiments. [45]

Different models were used: an atomic model, a coarse-grained model, and a colloidal model. The all-atom simulations show localized association of yttrium ions on the surface of HSA. Although solvent features are lost when using an amino acid level coarse-grained model, the localization of yttrium on the protein surface is well estimated. The study of the effective charge of the protein plus ions complex with increasing Y^{3+} concentration is in good agreement with reentrant condensation boundaries reported in the literature. [12]

The coarse-grained model was used to estimate the potential of mean force between two HSA molecules at different Y^{3+} concentrations. The results showed two phases, one where the increase in $[Y^{3+}]$ reduced the repulsion between proteins and promoted association (low Y^{3+} concentrations), and one where the increase in $[Y^{3+}]$ increased the interparticle repulsion (high Y^{3+} concentrations). The addition of NaCl suppressed those two effects, showing that they are driven by water-mediated electrostatic interactions. This is consistent with the reentrant condensation phenomenon reported in HSA/Y^{3+} systems.

The colloidal model was used to study the interactions of two spherical colloids representing HSA-like molecules. This approach enabled us to include all ions explicitly in a two-body system, which is more difficult and computationally costly to realize with coarse-grained models at high ion concentrations. The results show that taking the ions into account implicitly including the colloids counterions, implicitly without including the colloids counterions or explicitly, has a large influence on the interparticle forces at low salt concentration (0.525 mM yttrium), but essentially none at moderate salt concentration (6.5 mM yttrium).

Interesting further application of our simulation protocols, and particularly the coarse-grained model with a mix of explicit and implicit salt ions, would be the study of many-

body systems. Indeed, a number of SAXS experiments have been performed on protein and trivalent salt systems but the fitting of the spectra has for now been limited to analytical models (screened Coulomb potential and sticky hard spheres). [12,19,20,47] Spectra obtained from many-body simulation would be directly comparable to experimental spectra, and provide further information about the mechanisms underlying the charge reversal. More specifically, such simulations could explicitly include both trivalent ions and protein counter-ions while monovalent ions are included implicitly, which would account for the influence of counter-ion condensation on protein-protein interactions.

Acknowledgement

References

(1) Guldbrand, L.; Jonsson, B.; Wennerstrom, H.; Linse, P. Electrical Double Layer Forces. A Monte Carlo Study. *The Journal of Chemical Physics* **1984**, *80*, 2221.

(2) Kjellander, R.; Marcĕlja, S. Correlation and Image Charge Effects in Electric Double Layers. *Chemical Physics Letters* **1984**, *112*, 49–53.

(3) Grosberg, A. Y.; Nguyen, T. T.; Shklovskii, B. I. Colloquium : The Physics of Charge Inversion in Chemical and Biological Systems. *Reviews of Modern Physics* **2002**, *74*, 329–345.

(4) Quesada-Pérez, M.; González-Tovar, E.; Martín-Molina, A.; Lozada-Cassou, M.; Hidalgo-Álvarez, R. Overcharging in Colloids: Beyond the Poisson-Boltzmann Approach. *ChemPhysChem* **2003**, *4*, 234–248.

17

(5) Walker, H. W.; Grant, S. B. Factors Influencing the Flocculation of Colloidal Particles by a Model Anionic Polyelectrolyte. *Colloids and Surfaces A* **1996**, *119*, 229–239.

(6) Götting, N.; Fritz, H.; Maier, M.; von Stamm, J.; Schoofs, T.; Bayer, E. Effects of Oligonucleotide Adsorption on the Physicochemical Characteristics of a Nanoparticle-Based Model Delivery System for Antisense Drugs. *Colloid and Polymer Science* **1999**, *277*, 145–152.

(7) Kabanov, V.; Yaroslavov, A.; Sukhishvili, S. Interaction of Polyions with Cell-Mimetic Species: Physico-Chemical and Biomedical Aspects. *Journal of Controlled Release* **1996**, *39*, 173–189.

(8) Martín-Molina, A.; Quesada-Pérez, M.; Galisteo-González, F.; Hidalgo-Álvarez, R. Looking into Overcharging in Model Colloids through Electrophoresis: Asymmetric Electrolytes. *The Journal of Chemical Physics* **2003**, *118*, 4183.

(9) Wang, Y.; Kimura, K.; Huang, Q.; Dubin, P. L.; Jaeger, W. Effects of Salt on Polyelectrolyte-Micelle Coacervation. *Macromolecules* **1999**, *32*, 7128–7134.

(10) Kabanov, A. V.; Kabanov, V. A. DNA Complexes with Polycations for the Delivery of Genetic Material into Cells. *Bioconjugate Chemistry* **1995**, *6*, 7–20.

(11) Raspaud, E.; Chaperon, I.; Leforestier, A.; Livolant, F. Spermine-Induced Aggregation of DNA, Nucleosome, and Chromatin. *Biophysical Journal* **1999**, *77*, 1547–1555.

(12) Zhang, F.; Skoda, M.; Jacobs, R.; Zorn, S.; Martin, R.; Martin, C.; Clark, G.; Weggler, S.; Hildebrandt, a.; Kohlbacher, O. et al. Reentrant Condensation of Proteins in Solution Induced by Multivalent Counterions. *Physical Review Letters* **2008**, *101*, 3–6.

(13) Kubíčková, A.; Křížek, T.; Coufal, P.; Vazdar, M.; Wernersson, E.; Heyda, J.; Jungwirth, P. Overcharging in Biological Systems: Reversal of Electrophoretic Mobility of

Aqueous Polyaspartate by Multivalent Cations. *Physical Review Letters* **2012**, *108*, 186101.

(14) Pianegonda, S.; Barbosa, M. C.; Levin, Y. Charge Reversal of Colloidal Particles. *Europhysics Letters* **2005**, *71*, 831–837.

(15) Nguyen, T. T.; Grosberg, A. Y.; Shklovskii, B. I. Macroions in Salty Water with Multivalent Ions: Giant Inversion of Charge. *Physical Review Letters* **2000**, *85*, 1568–1571.

(16) Besteman, K.; Zevenbergen, M. A. G.; Heering, H. A.; Lemay, S. G. Direct Observation of Charge Inversion by Multivalent Ions as a Universal Electrostatic Phenomenon. *Physical Review Letters* **2004**, *93*, 170802.

(17) Peters, T. *All About Albumin: Biochemistry, Genetics, and Medical Applications*; Academic Press: San Diego, 1996.

(18) Zhang, F.; Weggler, S.; Ziller, M. J.; Ianeselli, L.; Heck, B. S.; Hildebrandt, A.; Kohlbacher, O.; Skoda, M. W. A.; Jacobs, R. M. J.; Schreiber, F. Universality of Protein Reentrant Condensation in Solution Induced by Multivalent Metal Ions. *Proteins* **2010**, *78*, 3450–3457.

(19) Wolf, M.; Roosen-Runge, F.; Zhang, F.; Roth, R.; Skoda, M. W.; Jacobs, R. M.; Sztucki, M.; Schreiber, F. Effective Interactions in Protein–Salt Solutions Approaching Liquid–Liquid Phase Separation. *Journal of Molecular Liquids* **2014**, *200*, 20–27.

(20) Jordan, E.; Roosen-Runge, F.; Leibfarth, S.; Zhang, F.; Sztucki, M.; Hildebrandt, A.; Kohlbacher, O.; Schreiber, F. Competing Salt Effects on Phase Behavior of Protein Solutions: Tailoring of Protein Interaction by the Binding of Multivalent Ions and Charge Screening. *The Journal of Physical Chemistry B* **2014**, *118*, 11365–11374.

(21) Zhang, F.; Zocher, G.; Sauter, A.; Stehle, T.; Schreiber, F. Novel Approach to Con-

trolled Protein Crystallization through Ligandation of Yttrium Cations. *Journal of Applied Crystallography* **2011**, *44*, 755–762.

(22) Zhang, F.; Roth, R.; Wolf, M.; Roosen-Runge, F.; Skoda, M. W. A.; Jacobs, R. M. J.; Stzucki, M.; Schreiber, F. Charge-Controlled Metastable Liquid–Liquid Phase Separation in Protein Solutions as a Universal Pathway towards Crystallization. *Soft Matter* **2012**, *8*, 1313–1316.

(23) Zhang, F.; Roosen-Runge, F.; Sauter, A.; Wolf, M.; Jacobs, R. M. J.; Schreiber, F. Reentrant Condensation, Liquid–Liquid Phase Separation and Crystallization in Protein Solutions Induced by Multivalent Metal Ions. *Pure and Applied Chemistry* **2014**, *86*, 191–202.

(24) Roosen-Runge, F.; Heck, B. S.; Zhang, F.; Kohlbacher, O.; Schreiber, F. Interplay of pH and Binding of Multivalent Metal Ions: Charge Inversion and Reentrant Condensation in Protein Solutions. *The Journal of Physical Chemistry B* **2013**, *117*, 5777–5787.

(25) Soraruf, D.; Roosen-Runge, F.; Grimaldo, M.; Zanini, F.; Schweins, R.; Seydel, T.; Zhang, F.; Roth, R.; Oettel, M.; Schreiber, F. Protein Cluster Formation in Aqueous Solution in the Presence of Multivalent Metal Ions – a Light Scattering Study. *Soft Matter* **2014**, *10*, 894–902.

(26) Wardell, M.; Wang, Z.; Ho, J. X.; Robert, J.; Ruker, F.; Ruble, J.; Carter, D. C. The Atomic Structure of Human Methemalbumin at 1.9 Å. *Biochemical and Biophysical Research Communications* **2002**, *291*, 813–819.

(27) Jorgensen, W. L.; Maxwell, D. S.; Tirado-Rives, J. Development and Testing of the OPLS All-Atom Force Field on Conformational Energetics and Properties of Organic Liquids. *Journal of the American Chemical Society* **1996**, *118*, 11225–11236.

(28) Bowron, D. T.; Diaz-Moreno, S. Local Structure Refinement of Disordered Material

Models: Ion Pairing and Structure in YCl3 Aqueous Solutions. *The Journal of Physical Chemistry B* **2007**, *111*, 11393–11399.

(29) Berendsen, H.; Postma, J.; van Gunsteren, W.; Hermans, J. In *Intermolecular Forces*; Pullman, B., Ed.; The Jerusalem Symposia on Quantum Chemistry and Biochemistry; Springer Netherlands, 1981; Vol. 14; pp 331–342.

(30) Leontyev, I.; Stuchebrukhov, A. Accounting for Electronic Polarization in Non-Polarizable Force Fields. *Physical Chemistry Chemical Physics* **2011**, *13*, 2613–26.

(31) Jungwirth, P.; Tobias, D. J. Specific Ion Effects at the Air/Water Interface. *Chemical Reviews* **2006**, *106*, 1259–81.

(32) Essmann, U.; Perera, L.; Berkowitz, M. L.; Darden, T.; Lee, H.; Pedersen, L. G. A Smooth Particle Mesh Ewald Method. *The Journal of Chemical Physics* **1995**, *103*, 8577.

(33) Nose, S. A Molecular Dynamics Method for Simulations in the Canonical Ensemble. *Molecular Physics* **1984**, *52*, 255–268.

(34) Parrinello, M.; Rahman, A. Polymorphic Transitions in Single Crystals: A New Molecular Dynamics Method. *Journal of Applied Physics* **1981**, *52*, 7182–7190.

(35) Hess, B.; Bekker, H.; Berendsen, H. J. C.; Fraaije, J. G. E. M. LINCS: A Linear Constraint Solver for Molecular Simulations. *Journal of Computational Chemistry* **1997**, *18*, 1463–1472.

(36) Hockney, R.; Goel, S.; Eastwood, J. Quiet High-Resolution Computer Models of a Plasma. *Journal of Computational Physics* **1974**, *14*, 148–158.

(37) Hess, B.; Kutzner, C.; van der Spoel, D.; Lindahl, E. GROMACS 4: Algorithms for Highly Efficient, Load-Balanced, and Scalable Molecular Simulation. *Journal of Chemical Theory and Computation* **2008**, *4*, 435–447.

(38) Forsman, J.; Nordholm, S. Polyelectrolyte Mediated Interactions in Colloidal Dispersions: Hierarchical Screening, Simulations, and a New Classical Density Functional Theory. *Langmuir* **2012**, *28*, 4069–4079.

(39) Kurut, A.; Persson, B. a.; Å kesson, T.; Forsman, J.; Lund, M. Anisotropic Interactions in Protein Mixtures: Self Assembly and Phase Behavior in Aqueous Solution. *The Journal of Physical Chemistry Letters* **2012**, *3*, 731–734.

(40) Lund, M. Ammonia in Saline Solutions. M.Sc. thesis, University of Copenhagen, 2001.

(41) Linse, P. Mean Force Between Like-Charged Macroions at High Electrostatic Coupling. *Journal of Physics: Condensed Matter* **2002**, *14*, 13449–13467.

(42) Wu, D.; Chandler, D.; Smit, B. Electrostatic Analogy for Surfactant Assemblies. *The Journal of Physical Chemistry* **1992**, *96*, 4077–4083.

(43) Stenqvist, B.; Thuresson, A.; Kurut, A.; Vácha, R.; Lund, M. Faunus A Flexible Framework for Monte Carlo Simulation. *Molecular Simulation* **2013**, *39*, 1233–1239.

(44) Martell, A. E.; Smith, R. M. *Critical Stability Constants - Volume 3: Other Organic Ligands*; Plenum Press: New York & London, 1977.

(45) Matsarskaia, O.; Braun, M. K.; Roosen-Runge, F.; Wolf, M.; Zhang, F.; Roth, R.; Schreiber, F. Cation-Induced Hydration Effects Cause Lower Critical Solution Temperature Behavior in Protein Solutions. *The Journal of Physical Chemistry B* **2016**, *120*, 7731–7736.

(46) Lund, M.; Jönsson, B. Driving Forces Behind Ion-Ion Correlations. *The Journal of Chemical Physics* **2006**, *125*, 236101.

(47) Sauter, A.; Zhang, F.; Szekely, N. K.; Pipich, V.; Sztucki, M.; Schreiber, F. Structural Evolution of Metastable Protein Aggregates in the Presence of Trivalent Salt Studied by (V)SANS and SAXS. *The Journal of Physical Chemistry B* **2016**, *120*, 5564–5571.

TOC Graphic

Double layer
Repulsion

Ion-ion correlation
Attraction

Over-charge
Repulsion

Non-Coulombic
Attraction

[**M**Cl$_3$]   [NaCl]